J. Fluid Mech. (2006), *vol.* 546, *pp.* 113–122. © 2005 Cambridge University Press
doi:10.1017/S0022112005007135 Printed in the United Kingdom

Bubbles in a viscous liquid: lattice Boltzmann simulation and experimental validation

By XAVIER FRANK, DENIS FUNFSCHILLING, NOËL MIDOUX AND HUAI Z. LI

Laboratoire des Sciences du Génie Chimique (UPR 6811 CNRS), ENSIC-INPL, 1, rue Grandville, BP 451, 54001 Nancy Cedex, France

(Received 20 May 2005 and in revised form 9 September 2005)

The dynamics of a single bubble rising in a viscous Newtonian fluid was investigated both experimentally by a particle image velocimetry (PIV) device and numerically using the free-energy-based lattice Boltzmann (LB) model. The rise velocity, bubble shape and flow field were considered for various bubble volumes in axisymmetric flow conditions. Experimentally, the flow measurements by the PIV device revealed the wake increasing with the bubble volume. Such an evolution is linked to the deformation of bubble shape from spherical for small bubbles to flattened at the bottom for large bubbles. The LB simulations compare satisfactorily with our experimental data for both the bubble shape and drag coefficient over the range of Reynolds number ($0.033 \leqslant Re \leqslant 1.8$). With a more extended flow structure around the bubble compared to experiments, the two-dimensional approach shows some limitations in its quantitative description. Fully three-dimensional simulations are necessary, especially for bigger bubbles with $Re > 1.8$.

1. Introduction

The motion of bubbles in a liquid has been the focus of both academic and practical interest for a long time. A huge literature has been generated (Clift, Grace & Weber 1978; Sadhal, Ayyaswamy & Chung 1997). The central problem is the relationship between the rise velocity, bubble shape due to the interface deformation and flow field. For example, the deformation of a bubble rising in an inviscid or viscous liquid has been experimentally studied by Hnat & Buckmaster (1976), Bhaga & Weber (1981) and Maxworthy *et al.* (1996). Approximate theoretical solutions have been developed in the limit of very small deformation of bubbles for either high (Moore 1959) or low (Taylor & Acrivos 1964) Reynolds numbers.

In the case of very viscous fluids, there are also numerous applications that require knowledge of the rise of bubbles either individually or in an interacting cloud, such as volcanic eruption (Morrissey & Chouet 1997; Rust, Manga & Cashman 2003), metallurgy (Xie & Oeters 1994), wastewater treatment (Cui, Chang & Fane 2003) and fermentation (Kilonzo & Margaritis 2004). Aside from the terminal velocity usually estimated by empirical correlations (Rodrigue 2001), we know little about the flow field around a bubble in such fluids.

The lattice Boltzmann (LB) method, emerging from theoretical physics studies on lattice gas automata, has recently become an interesting alternative to the classical computational fluid dynamics. In a multiphase flow context, LB has been successfully applied to various classical problems, like bubbly flows in narrow channel (Yang,

https://doi.org/10.1017/S0022112005007135 Published online by Cambridge University Press

Palm & Sehgal 2002), phase transition (Martys & Douglas 2001) and bubbles rising in non-Newtonian fluids (Frank & Li 2005). Sankaranarayanan *et al.* (2002) focused on the computation of drag and virtual mass forces in a regular array of uniformly sized bubbles with a Reynolds number ranging from 50 to 400, and observed no difference between two- and three-dimensional simulations. In this paper, we present an investigation of axisymmetric bubble motion in a viscous Newtonian fluid both by the LB scheme and experimentally. For small Reynolds number, both the axisymmetric bubble shape and flow structure are particularly suitable for experimental investigation and validation of the LB method. To our best knowledge, there exist neither LB simulation nor flow field measurements by particle image velocimetry (PIV) around a rising bubble for small Reynolds number except for the qualitative visualization by Bhaga & Weber (1981) through the hydrogen bubble tracer technique.

2. Lattice Boltzmann approach

Fluids are described statistically at the microscopic level within the framework of the lattice Boltzmann scheme. Particle probability density functions (PPDF) $f_i(\boldsymbol{r}, t)$ represent the number of particles having velocity $\boldsymbol{c}_i$ at point $\boldsymbol{r}$ and time t. The LB approach consists of computing the evolution of $f_i(\boldsymbol{r}, t)$, due to advection and collisions of particles. Particles can move only on the nodes of a lattice, the classical D2Q9 lattice is used in the present work, which is a two-dimensional lattice involving nine particle velocities $\boldsymbol{c}_i$. The main macroscopic quantities are deduced from the PPDF.

Several LB approaches have been proposed in the literature for modelling multiphase flows (Yang *et al.* 2002; Nourgaliev *et al.* 2003), but there is no consensus. The pseudo-potential approach developed by Shan & Chen (1994) stems from pairwise molecular interactions. The physical meaning is that at each lattice site, the net force experienced by a particle of a species is the sum of the momentum exchanges with particles of all other species in the neighbourhood. The attractive features of this model are the ease implementation and the spontaneous separation between phases. Unfortunately, some numerical fluctuations such as spurious velocities arise near the interface due to the lack of local momentum conservation. An improvement in the thermodynamic consistency was realized in the free-energy approach with a pressure tensor $P_{\alpha\beta}$ (Swift, Osborn & Yeomans 1995). The main merit of this model is that the fluid must reach the right thermodynamic equilibrium directly within the framework of the correct thermodynamic equation of state. In particular, the free-energy approach leads to significant reduction of the velocity fluctuations near the interface and ensures a satisfactory isotropy of the surface tension. This second advantage is particularly useful for the modelling of the rise of a bubble in a fluid. There are however criticisms related to the rigorous thermodynamic consistency as well as to the possible exposure to higher-order lattice artefacts, but these shortcomings are likely to be problem-dependent. In the case of the rise of a bubble in a viscous Newtonian fluid, we did not experience such difficulties. To conserve the Galilean invariance, the LB scheme used in this work is for a two-component and binary system.

In the present study, air bubbles are assimilated as drops of fluid A in a viscous liquid B. The densities of components A and B of the binary fluid are respectively ρ_A and ρ_B; $\rho = \rho_A + \rho_B$ is the total density and $\Delta\rho = \rho_A - \rho_B$ the density difference. Macroscopic fields, ρ, $\Delta\rho$ and $\boldsymbol{u}$, are expressed as functions of $f_i(\boldsymbol{r}, t)$ and $g_i(\boldsymbol{r}, t)$ by

$$\rho = \sum_i f_i, \quad \rho u_\alpha = \sum_i f_i c_{i\alpha}, \quad \Delta\rho = \sum_i g_i. \tag{1.1a–c}$$

https://doi.org/10.1017/S0022112005007135 Published online by Cambridge University Press

A quantity τ_f is linked to spatial step δx, time step δt, fluid viscosity η and fluid density ρ_F by $\eta = \tau_f \rho_F \delta t c_s^2 c^2$ (Nourgaliev *et al.* 2003), where $c = \delta x/\delta t$ and c_s is the pseudo-sound speed in lattice units. τ_g is another dimensionless time parameter equal to 1 here. With such definitions, we can then compute the time step:

$$\delta t = \frac{\rho_F \tau_f c_s^2 \delta x^2}{\eta}. \tag{1.2}$$

Velocities in real units are deduced from the lattice units via $U_\alpha = c u_\alpha$. As the vector $\boldsymbol{a}(\boldsymbol{r}, t)$ is an external acceleration, distributions f_i and g_i obey the so-called lattice Bhatnagar–Gross–Krook (LBGK) equation

$$f_i(\boldsymbol{r} + \boldsymbol{c}_i, t+1) - f_i(\boldsymbol{r}, t) = -\frac{1}{\tau_f}\left(f_i - f_i^{eq}\right) + \frac{\boldsymbol{a}\cdot(\boldsymbol{c}_i - \boldsymbol{u})}{c_s^2} f_i^{eq}, \tag{1.3a}$$

$$g_i(\boldsymbol{r} + \boldsymbol{c}_i, t+1) - g_i(\boldsymbol{r}, t) = -\frac{1}{\tau_g}\left(g_i - g_i^{eq}\right). \tag{1.3b}$$

Equilibrium values of the PPDF are deduced from macroscopic quantities:

$$\sum_i f_i^{eq} = \rho, \quad \sum_i f_i^{eq} c_{i\alpha} = \rho u_\alpha, \quad \sum_i f_i^{eq} c_{i\alpha} c_{i\beta} = \rho u_\alpha u_\beta + P_{\alpha\beta}, \tag{1.4a–c}$$

$$\sum_i g_i^{eq} = \Delta\rho, \quad \sum_i g_i^{eq} c_{i\alpha} = \Delta\rho u_\alpha, \quad \sum_i g_i^{eq} c_{i\alpha} c_{i\beta} = \Delta\rho u_\alpha u_\eta + \Delta\mu\delta_{\alpha\beta}. \tag{1.4d–f}$$

The chemical potential difference $\Delta\mu$ and the pressure tensor $P_{\alpha\beta}$ are defined by the well-known expressions

$$P_{\alpha\beta} = P\delta_{\alpha\beta} + \kappa(\partial_\alpha\rho\partial_\beta\rho + \partial_\alpha\Delta\rho\partial_\beta\Delta\rho), \tag{1.5a}$$

$$P = \rho c_s^2 - \kappa(\rho\,\partial_\alpha\partial_\alpha\rho + \Delta\rho\,\partial_\alpha\partial_\alpha\Delta\rho) - \tfrac{1}{2}\kappa(|\partial_\alpha\rho|^2 + |\partial_\alpha\Delta\rho|^2), \tag{1.5b}$$

$$\Delta\mu = \tfrac{1}{2}c_s^2 \ln\left(\frac{\rho + \Delta\rho}{\rho - \Delta\rho}\right) - \tfrac{1}{2}\lambda\frac{\Delta\rho}{\rho} - \kappa\,\partial_\alpha\partial_\alpha\Delta\rho. \tag{1.5c}$$

For the phase interaction parameter $\lambda > 2c_s^2$, the above scheme leads to spontaneous phase segregation (Swift *et al.* 1995). As a consequence, the interface does not require specific numerical tracking. Within the framework of the free-energy scheme, the parameter κ is closely linked to the surface tension. However, a shortcoming, is that there is still no rigorous physical understanding to allow its theoretical prediction for various gas–liquid systems. In the case of air bubbles rising in glycerol, we have made LB simulations with various values of κ to compare with the simplest visual parameter, which is the bubble's shape. For quite different bubble volumes ranging from spherical to spherical cap shape, a constant and fixed value $\kappa = 0.02$ was found to be the best for describing the bubble's shape. From a physical point of view, this requires further investigation both theoretically and experimentally.

The external force $\boldsymbol{a}$ depends mainly on $\Delta\rho$: $\boldsymbol{a} = -\boldsymbol{g}$ in gas, and $\boldsymbol{a} = \boldsymbol{0}$ in liquid, the $\boldsymbol{g}$ vector being gravity in dimensionless form.

To initiate the simulation, spherical bubbles of different volumes are placed at the bottom of a box 200 nodes wide and 400 nodes high and representing a liquid column of 7 cm large and 14 cm height. This is the compromise that we found between a satisfactory comparison with experimental data and acceptable computation time on a PC for the considered range of bubble volumes. To isolate the bubble, at the left and right boundaries solid wall boundary conditions are applied as in the experimental case, as well as at the top and bottom. The simulation section covered by the LB nodes is high

https://doi.org/10.1017/S0022112005007135 Published online by Cambridge University Press

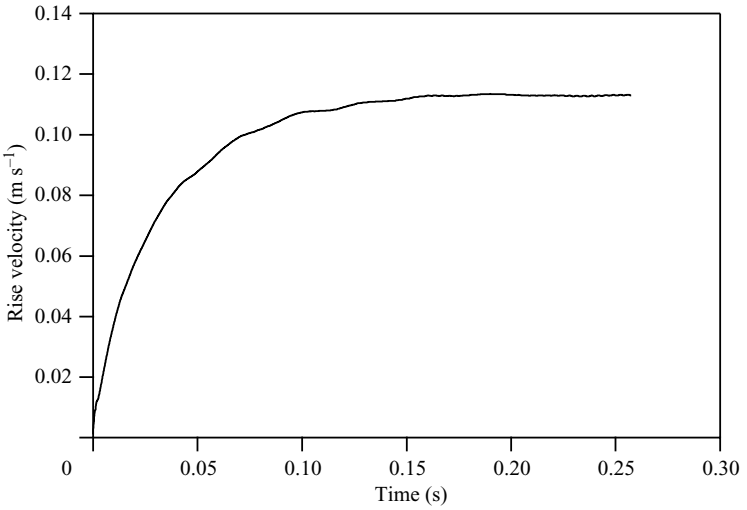


FIGURE 1. LB simulation: variation of the rise velocity towards an asymptotic terminal value for a bubble of $V_0 = 1100\,\mathrm{mm}^3$.

enough for a bubble to reach a stationary rise regime before approaching the top and sufficiently wide to avoid possible wall effects under deformable interface conditions.

After thermodynamic equilibrium is obtained, iterations with buoyancy are performed and useful data (velocity field, bubble shape) are stored. For each simulation, the stationary rise regime is effectively reached. In figure 1, the evolution of the rise velocity is illustrated for a bubble of volume $V_0 = 1100\,\mathrm{mm}^3$ and the terminal rise velocity can be easily determined. Another example is shown in figure 2 for the variation of the bubble shape from an initial sphere to a stationary shape with a flattened bottom. This is accompanied by the modification of the flow field around the bubble.

3. Experimental setup

The experiments were conducted in a Plexiglas cylindrical tank (0.24 m diameter and 1 m height), enclosed by a square duct (0.33 m) to eliminate optical distortions for visualization as well as to keep the liquid temperature inside the cylindrical tank at 293 K. Air bubble generation was through an orifice of 1 mm diameter, submerged in the liquid in the centre of the bottom section of the tank. An electronic valve of rapid response controlled by a PC allowed injection of individual bubbles of a desired volume by varying the open duration of the valve or the air pressure inside a $4 \times 10^{-3}\,\mathrm{m}^3$ reservoir. The bubble rise velocity was measured by both optical laser and photodiodes probes placed at different heights and a particle image velocimetry (PIV, Dantec Dynamics) device and bubble shapes were extracted from video recording and digitization.

The viscous Newtonian fluid used in this work was 99.5 % glycerol (Dow Europe) with some water trace due to humidity. Its density was $1261\,\mathrm{kg\,m}^{-3}$. A Rheometrics Fluid Spectrometer RFS II (Rheometric Scientific) was employed to measure the fluid viscosity, which was 1.20 Pa s, and the air–glycerol surface tension measured on a Krüss Tensiometer K100 was $62\,\mathrm{mN\,m}^{-1}$.

The flow field was measured by means of a PIV device composed of two YAG laser, a camera, a cross-correlator and a computer. In the viscous glycerol solution,

https://doi.org/10.1017/S0022112005007135 Published online by Cambridge University Press

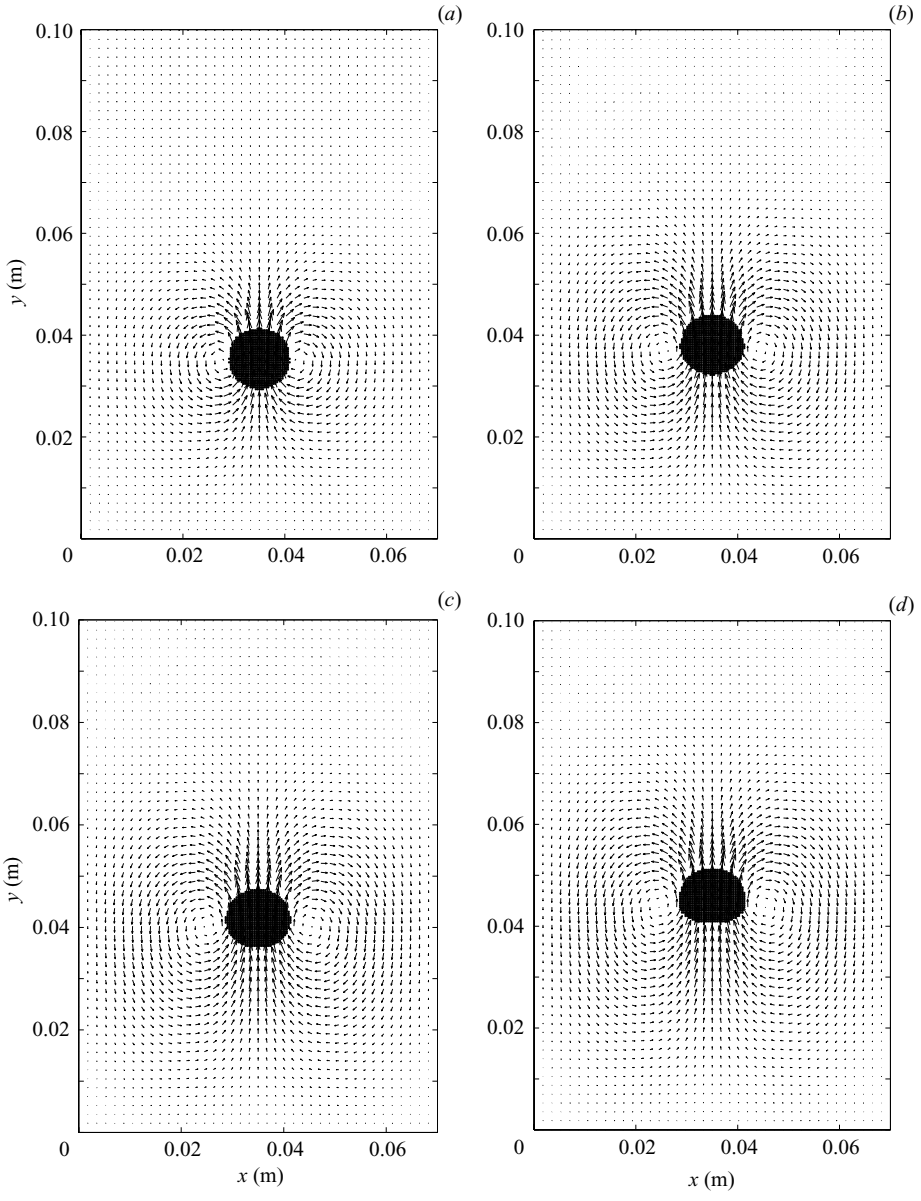


FIGURE 2. LB simulation of the transient rise of a bubble of volume $V_0 = 900\,\mathrm{mm}^3$ initially spherical at rest. (*a*) $t = 0.021$ s, (*b*) $t = 0.065$ s, (*c*) $t = 0.108$ s, (*d*) $t = 0.151$ s in the terminal rise regime.

bubbles were perfectly axisymmetric, and displayed neither shape nor trajectory oscillations within the range of bubble volumes studied. The flow field was also found to be axisymmetric. Hence, two-dimensional measurements in a plane crossing the symmetry axis of a rising bubble lead to a complete knowledge of the flow field around the bubble. The fluid was injected with fluorescent polymer beads of 75 μm diameter and comparable density as seeding particles. An orange filter placed in front of the camera eliminated the reflections of the lasers on the bubbles and allowed only the passage of the fluorescent light from the seeding particles. The two laser sheets

https://doi.org/10.1017/S0022112005007135 Published online by Cambridge University Press

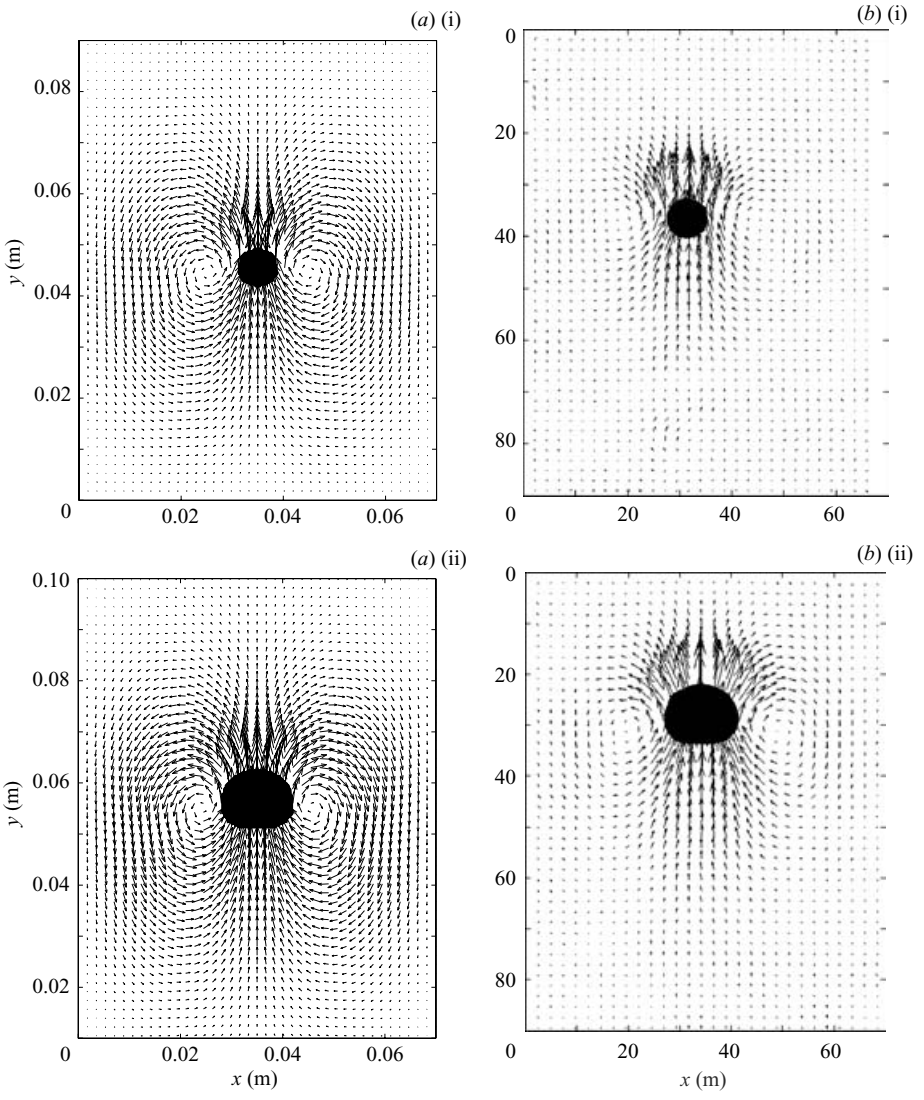


FIGURE 3. Flow field in glycerol around a bubble of volume (i) $V_0 = 200\,\mathrm{mm}^3$ and (ii) $V_0 = 1100\,\mathrm{mm}^3$. (*a*) LB simulations with the computed bubble shape. (*b*) PIV measurements with the real bubble shape.

crossed the vertical symmetry axis of the bubble. The camera, placed perpendicular to the laser sheets, took two successive images, each at the maximum intensity of the laser impulse. These images were divided into several thousand small interrogation areas of 32×32 pixels. A cross-correlation was then performed on the two corresponding interrogation areas to give the instantaneous flow field.

4. Results

As shown in figure 3 and figure 4, experimental flow fields are in qualitative agreement with the LB simulations for a small and large bubble. Note that the magnitude of the velocity fields of the experiments and the LB simulation is comparable. Both exhibit an upward flow at the top and bottom of the bubble,

https://doi.org/10.1017/S0022112005007135 Published online by Cambridge University Press

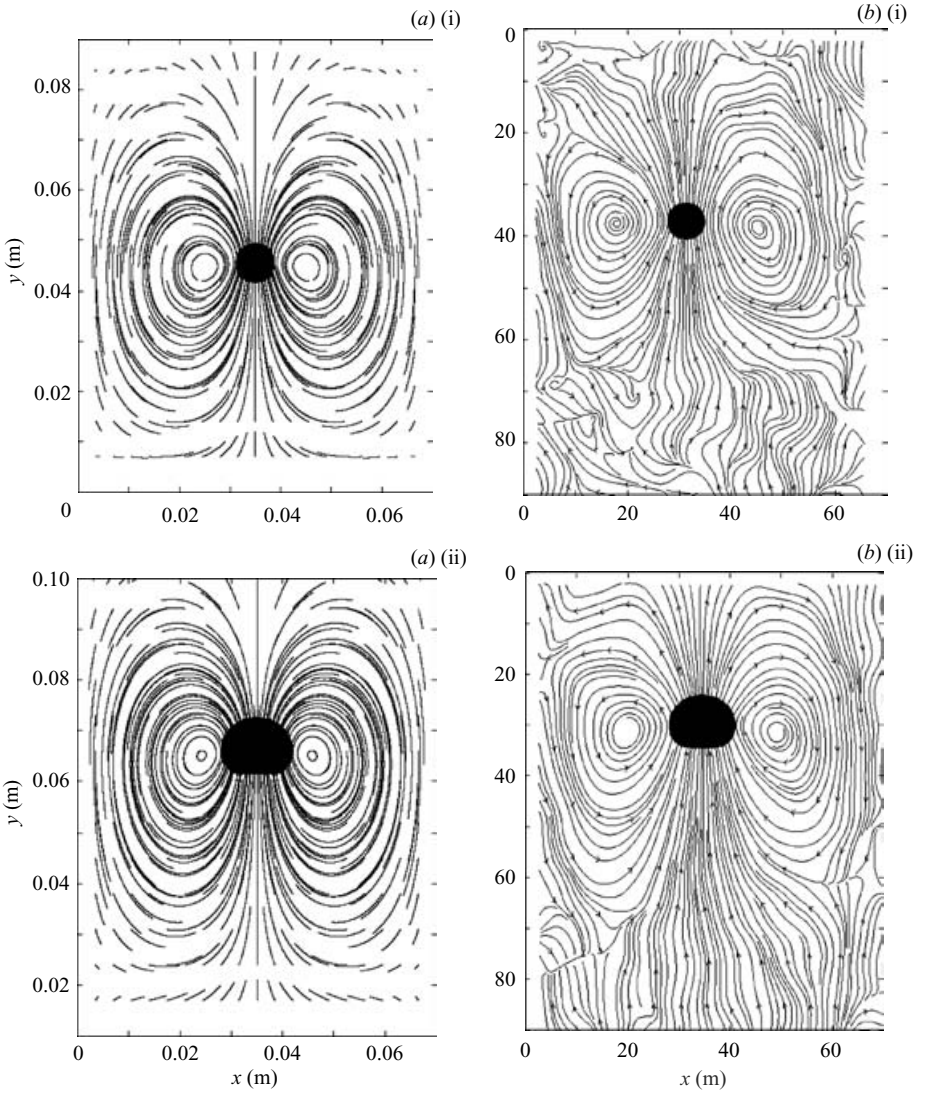


FIGURE 4. Streamlines in glycerol around a bubble of volume (i) $V_0 = 200\,\mathrm{mm}^3$ and (ii) $V_0 = 1100\,\mathrm{mm}^3$. (*a*) LB simulations with the computed bubble shape. (*b*) PIV measurements with the real bubble shape.

downward flow occurring at the edge of the column due to mass conservation. Streamlines of the flow around a rising bubble confirm the recirculation between the upward flow in the front of bubbles and that in the wake at the side of the bubble. This recirculation region expands space with an increase of the bubble volume.

These flow features can be closely linked to the results on the bubble shape (figure 5) where the experimental visualization compares well with the LB simulations. The experimental Reynolds, Eötvös and Weber numbers as well as the simulation Reynolds number are also indicated in figure 5. In spite of its relationship with the classical surface tension, the parameter κ in the LB scheme cannot allow a straightforward estimation for the Eötvös and Weber numbers. For small bubbles, the shape is spherical, and for larger bubbles the bottom is progressively flattened

https://doi.org/10.1017/S0022112005007135 Published online by Cambridge University Press

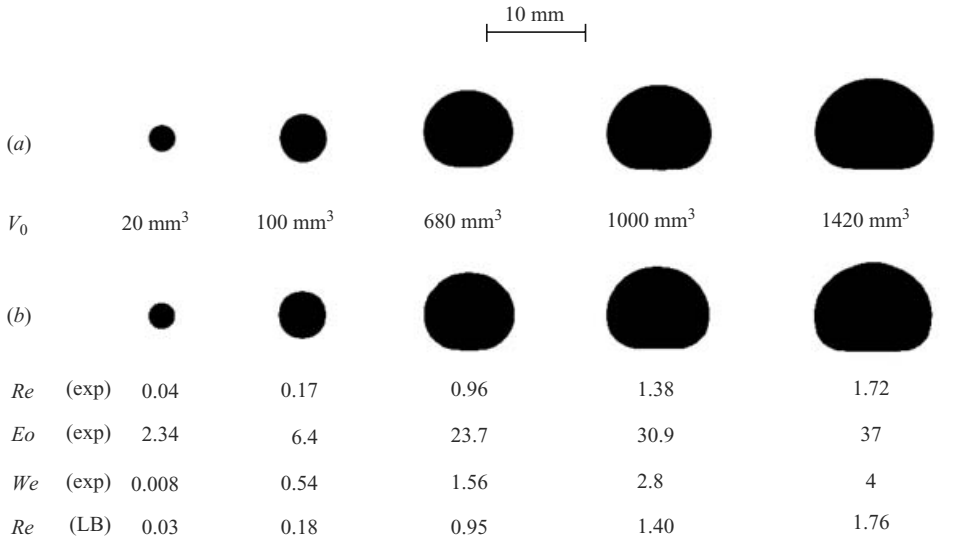


FIGURE 5. Some examples of the variation of bubble shape in glycerol with the bubble volume V_0, Re, Eo and We from experiments, and Re from LB simulations; (a) experimental visualization; (b) LB computation.

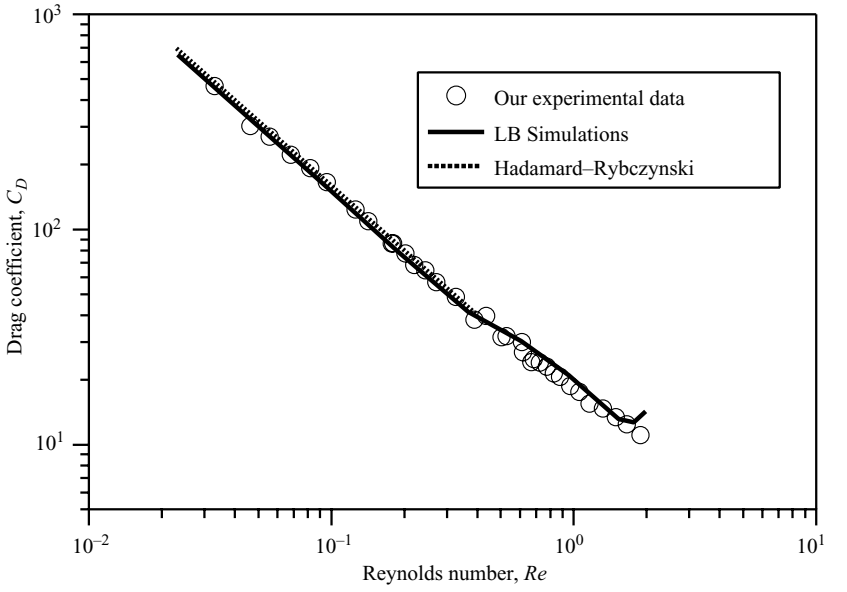


FIGURE 6. Variation of the drag coefficient C_D with the Reynolds number Re in glycerol.

whereas the top remains spherical, as found by other workers. The bubble's shape deformation can be regarded as a natural consequence of the fluid flow fields as the upward flow in the wake and the recirculation at the side are both increased with an increase of the bubble volume and flatten the bubble bottom towards a spherical cap shape. The effect of the shape deformation on the rise velocity of bubbles can be established by comparing the drag coefficient predicted by the LB approach with our experimental data obtained in the viscous glycerol fluid (figure 6). The theoretical

https://doi.org/10.1017/S0022112005007135 Published online by Cambridge University Press

drag coefficient was directly determined from the rise velocity computed by the LB simulation. For $Re \leqslant 0.40$ corresponding to a bubble volume of $V_0 \leqslant 200\,\mathrm{mm}^3$ where the Hadamard–Rybczynskis drag expression is valid for a spherical bubble, the LB simulations compare satisfactorily with the experimental results. Above this critical value, accompanying the beginning of the shape deformation, the LB simulations are still in reasonable agreement with the experimental data but with increasing deviation.

As numerous multiphase flow situations exist where the fluid dynamics can be approximated as axisymmetric (Eggers 1997; Sussman & Smereka 1996), a two-dimensional approach is clearly a good approximation for three-dimensional phenomena. In particular, the working fluid in this study is very viscous with a Morton number of 67.7, and the two-dimensional LB simulation compares satisfactorily with the experiments, especially for the drag coefficient, which is a mean description, and for the bubble shape, which is not far from spherical. However, local differences exists between the simulation and experiments in both flow field and streamlines as shown in figure 3 and figure 4: the simulated flow structure is more extended than the two-dimensional measurements by the PIV device. This can be attributed to the macroscopic conservation laws such as for mass and momentum within the two-dimensional framework. Even for the drag coefficient, a deviation occurs for $Re > 1.8$ as the axisymmetric assumption is no longer valid (figure 6). In this case, a three-dimensional LB approach with parallel computation should be employed. In particular, a three-dimensional approach is essential for a study on the interactions and coalescence between bubbles with noticeable shape evolution and non-symmetric wake structure. This is an avenue we are currently exploring both experimentally by PIV measurements and numerically by the LB approach.

5. Conclusion

In summary, the lattice Boltzmann simulation captures the main features of the flow field, shape and rise velocity of bubbles in a viscous Newtonian fluid. These results are validated by a PIV device for the flow fields, camera visualization for the bubble shape and terminal velocity measurements. However, the two-dimensional LB simulations are limited to bubbles of a terminal rise Reynolds number under 1.8 to maintain the axisymmetric flow conditions. The apparent inadequacy of a two-dimensional approach is also obvious in the detailed quantitative comparison with experimental flow fields around a bubble. We are currently conducting fully three-dimensional studies for large bubbles and in particular for in-line interactions and coalescence between bubbles. For physical scales, we are also performing experiments in other fluids of varying viscosity and surface tension.

REFERENCES

Bhaga, D. & Weber, M. E. 1981 Bubbles in viscous liquids: shapes, wakes and velocities. *J. Fluid Mech.* **105**, 61–85.

Clift, R., Grace, J. R. & Weber, M. E. 1978 *Bubbles, Drops and Particles*. Academic.

Cui, Z. F., Chang, S. & Fane, A. G. 2003 The use of gas bubbling to enhance membrane processes. *J. Membrane Sci.* **221**, 1–35.

Eggers, J. 1997 Nonlinear dynamics and breakup of free-surface flows. *Rev. Mod. Phys.* **69**, 865–929.

Frank, X. & Li, H. Z. 2005 Complex flow around a bubble rising in a non-Newtonian fluid. *Phys. Rev.* E **71**, 036309.

Hnat, J. G. & Buckmaster, J. D. 1976 Spherical cap bubbles and skirt formation. *Phys. Fluids* **19**, 182–194.

https://doi.org/10.1017/S0022112005007135 Published online by Cambridge University Press

Kilonzo, P. M. & Margaritis, A. 2004 The effects of non-Newtonian fermentation broth viscosity and small bubble segregation on oxygen mass transfer in gas-lift bioreactors: a critical review. *Biochem. Engng J.* **17**, 27–40.

Martys, N. S. & Douglas, J. F. 2001 Critical properties and phase separation in lattice Boltzmann fluid mixtures. *Phys. Rev.* E **63**, 031205.

Maxworthy, T., Gnann, C., Krten, M. & Durst, F. 1996 Experiments on the rise of air bubbles in clean viscous liquids. *J. Fluid Mech.* **321**, 421–441.

Moore, D. W. 1959 The rise of a gas bubble in a viscous liquid. *J. Fluid Mech.* **6**, 113–130.

Morrissey, M. M. & Chouet, B. A. 1997 Burst Conditions of explosive volcanic eruptions recorded on microbarographs. *Science* **275**, 1290–1293.

Nourgaliev, R. P., Dinh, T. N., Theofanous, T. G. & Joseph, D. 2003 The lattice Boltzmann equation method: theoretical interpretation, numerics and implications. *Intl J. Multiphase Flow* **29**, 117–169.

Rodrigue, D. 2001 Generalized correlation for bubble motion. *AIChE J.* **47**, 39–44.

Rust, A. C., Manga, M. & Cashman, K. V. 2003 Determining flow type, shear rate and shear stress in magmas from bubble shapes and orientations. *J. Volcan. Geotherm. Res.* **122**, 111–132.

Sadhal, S. S., Ayyaswamy, P. S. & Chung, J. N. 1997 *Transport Phenomena with Drops and Bubbles.* Springer.

Sankaranarayanan, K., Shan, X., Kevrekidis, I. G. & Sundaresan, S. 2002 Analysis of drag and virtual mass forces in bubbly suspensions using an implicit formulation of the lattice Boltzmann method. *J. Fluid Mech.* **452**, 61–96.

Shan, X. & Chen, H. 1994 Simulation of nonideal gases and liquid-gas phase transitions by the lattice Boltzmann equation. *Phys. Rev.* E **49**, 2941–2948.

Sussman, M. & Smereka, P. 1996 Axisymmetric free boundary problems. *J. Fluid Mech.* **341**, 269–294.

Swift, M. R., Osborn, W. R. & Yeomans, J. M. 1995 Lattice Boltzmann simulation of nonideal fluids. *Phys. Rev. Lett.* **75**, 830–833.

Taylor, T. D. & Acrivos, A. 1964 On the deformation and drag of a falling viscous drop at low Reynolds number. *J. Fluid Mech.* **18**, 466–476.

Xie, Y. & Oeters, F. 1994 Measurements of bubble plume behaviour and flow velocity in gas stirred liquid Woods metal with an eccentric nozzle position. *Steel Res.* **65**, 315–319.

Yang, Z. L., Palm, B. & Sehgal, B. R. 2002 Numerical simulation of bubbly two-phase flow in a narrow channel. *Intl J. Heat Mass Transfer* **45** 631–639.

https://doi.org/10.1017/S0022112005007135 Published online by Cambridge University Press